HOKKAIDO UNIVERSITY

Title	Smooth Interfacial Scavenging for Resistive Switching Oxide via the Formation of Highly Uniform Layers of Amorphous TaOx
Author(s)	Tsurumaki-Fukuchi, Atsushi; Nakagawa, Ryosuke; Arita, Masashi; Takahashi, Yasuo
Citation	ACS Applied Materials & Interfaces, 10(6), 5609-5617 https://doi.org/10.1021/acsami.7b15384
Issue Date	2018-01-22
Doc URL	http://hdl.handle.net/2115/79115
Rights	This document is the Accepted Manuscript version of a Published Work that appeared in final form in ACS applied materials & interfaces, copyright c American Chemical Society after peer review and technical editing by the publisher. To access the final edited and published work see https://pubs.acs.org/doi/10.1021/acsami.7b15384.
Type	article (author version)
File Information	ACS applied materials & interfaces2018_Fukuchi-1.pdf

Instructions for use

Hokkaido University Collection of Scholarly and Academic Papers : HUSCAP

This document is the Accepted Manuscript version of a Published Work that appeared in final form in *ACS Applied Materials & Interfaces*, copyright © American Chemical Society after peer review and technical editing by the publisher. To access the final edited and published work see http://pubs.acs.org/articlesonrequest/AOR-atz8rTp8TdakmtpqKjhr.

Smooth Interfacial Scavenging for Resistive Switching Oxide via the Formation of Highly Uniform Layers of Amorphous TaO_x

Atsushi Tsurumaki-Fukuchi, Ryosuke Nakagawa, Masashi Arita, and Yasuo Takahashi*

Graduate School of Information Science and Technology, Hokkaido University, Sapporo, Hokkaido 060-0814, Japan

KEYWORDS: oxygen defect, scavenging layer, tantalum oxide, $SrTiO_3$, resistive switching

ABSTRACT: We demonstrate that the inclusion of a Ta interfacial layer is a remarkably effective strategy for forming interfacial oxygen defects at metal/oxide junctions. The insertion of an interfacial layer of reactive metal, i.e., a "scavenging" layer, has been recently proposed as a way to create a high concentration of oxygen defects at an interface in redox-based resistive switching devices, and growing interest has been given to the underlying mechanism. Through structural and chemical analyses of Pt/metal/$SrTiO_3$/Pt structures, we reveal that the rate and amount of oxygen scavenging is not directly determined by the formation free energies in the oxidation reactions of the scavenging metal and unveil the important roles of the oxygen diffusibility. Active oxygen scavenging and highly uniform oxidation via scavenging are revealed for a Ta interfacial layer with high oxygen diffusibility. In addition, the Ta scavenging layer is shown to exhibit a highly uniform structure and to form a very flat interface with $SrTiO_3$, which are advantageous for the fabrication of a steep metal/oxide contact.

INTRODUCTION

Defect formation at metal/oxide interfaces is gaining increasing importance in electronics because of its important effects on electronic properties and the emergence of rich interfacial phenomena. Because the fabrication of a metal/oxide contact is intrinsically accompanied by changes in the local oxygen concentrations (or valence state of metal ions) via interfacial redox reactions,[1] its control is essential for fabricating desired contacts in oxide devices. In addition, recent investigations have revealed that oxygen defects at metal/oxide interfaces can provide various functionalities to the junctions, such as the generation of two-dimensional carriers,[2]

modulation of contact resistance,[3] and interfacial magnetism.[4,5] Encouraged by these findings, a method for controlled formation of oxygen defects is being explored.

In the recent developments of valence-change resistive switching memory, many efforts have been directed toward interfacial defect formation. In resistive switching devices, oxygen defects serve to modify the carrier concentrations in the insulating layer and mediate reversible changes in the resistance, which lead to their operations as nonvolatile memory[6,7] or neuromorphic devices.[8] To achieve the locally high concentration of oxygen defects required for these operations, many methods have been employed to create oxygen defects, such as aliovalent cation doping, thermal annealing in reducing conditions, and the use of a reactive metal electrode.[6,7] In addition to these methods, a new technique for interfacial defect formation has been recently proposed for resistive switching oxides based on the insertion of a thin (~10 nm) metal layer at the interface between the inert electrode (Pt or Au) and oxide.[9–15] The interfacial layer, termed a "scavenging" layer, has been assumed to act as a reservoir of oxygen defects through electrochemical reactions with the oxide layer and to improve the reliability of resistive switching devices by stabilizing the reduced valence state of the oxide.[10,11] In addition, the use of a scavenging layer has enabled advanced operations of resistive switching devices, such as the induction of quantized conductance[16] and the fabrication of a neuromorphic network[17] or flexible memory array.[18,19]

In many works, the mechanism of oxygen scavenging has been discussed based on the chemical reactivity between the scavenging metal and oxygen, with the formation free energy of the reaction product oxide being used as the key parameter.[10–12,14,15,18,20–22] A recent theoretical study[11] proposed that the defect formation energy in the oxide, which determines the rate of the oxygen scavenging reaction, is dependent on the oxide formation energy of the scavenging metal

and that metals with high formation free energies (e.g., Al, Hf, and Ti) are effective in improving the switching endurance. Based on these assumptions, Al or Ti have been commonly used as the scavenging material in the fabrication of resistive switching devices.[9,10,16–21] However, oxygen scavenging by metal layers remains a poorly understood phenomenon because of the complex interfacial motion of oxygen. To optimize the properties of the scavenging layer and achieve smooth defect formation, detailed investigations of the mechanism are needed.

In fact, recent experimental studies have revealed that a characteristic layer of intermediate oxide is formed at various metal/oxide interfaces using Ta, Hf, Ti, and their oxides.[23–26] These studies have demonstrated that the interfacial oxide can generally be formed both at the homoatomic and heteroatomic interfaces,[25] and plays important roles in the resistive switching operations.[24,25] These studies have also suggested that the redox reactions at the metal/oxide interfaces occur through the reactions of the intermediate oxide, and the formation is possible even when it is energetically unfavorable in the bulk formation free energy.[15,25] These facts suggest that the rate of oxygen scavenging is not simply determined from the formation free energy for the oxide of scavenging metal, and may have a very different material dependence based on the behavior of interfacial reactions.

In this study, we investigate the effects of interfacial scavenging layers on the electrical properties and defect distributions of amorphous $SrTiO_3$ (STO) thin films. We inserted various metal layers at the top interface of Pt/STO/Pt structures, and the structure and oxygen distributions were analyzed using high-resolution transmission electron microscopy (HRTEM) and energy-dispersive X-ray spectroscopy (EDX). We observed that the transport properties of the STO structures were strongly affected by the scavenging material (M), and the occurrence of active oxygen scavenging was suggested for the structures with M = Ta. Because Ta has a

relatively large (less reactive) formation free energy for the stable oxide, our results show that the mechanism of the interfacial reactions have an important impact on the oxygen scavenging phenomenon at the metal/oxide interface. TEM/EDX analysis revealed the highly uniform structure and uniform internal oxygen distributions of the Ta scavenging layers, which formed a flat interface with STO. A model for active oxygen scavenging at the Ta/STO interface was proposed based on the experimental results.

EXPERIMENTAL METHODS

To evaluate the interfacial scavenging effects, we fabricated test structures of Pt(100 nm)/M(*d* nm)/STO(100 nm)/Pt(100 nm) (inset of Figure 1a) on Ti(10 nm)/SiO_2/Si substrates using RF sputtering, where the material (M) and thickness (*d*) of the scavenging layer were varied as M = Al, Ti, Zr, and Ta and *d* = 0–50 nm, respectively. Pure metal targets (for the Pt and M layers) and a $SrTiO_3$ target (for the STO layer) were used for the depositions, and all the layers were deposited at room temperature in an Ar atmosphere. Also in the subsequent fabrication steps, no thermal annealing process was performed for the structures. After the depositions of the Pt bottom electrode and STO layer, an interfacial metal layer of M and a top electrode of Pt were deposited through a shadow mask to form square-shaped electrodes with dimensions of 100 μm × 100 μm. The effects of the scavenging layers on the transport properties were evaluated based on measurements of the current–time (*I–t*) and current–voltage (*I–V*) characteristics using a B1500 semiconductor parameter analyzer (Keysight Co, Santa Rosa, CA, USA) by applying voltages from the top Pt electrode and grounding the bottom Pt electrode. Structural characterization and chemical analysis of the devices were performed using HRTEM and EDX

on a Titan 3 G2 60–300 (FEI, Hillsboro, OR, USA). The morphologies of the deposited layers were investigated using atomic force microscopy (AFM) with a Nanocute (Hitachi High-Technologies Co, Tokyo, Japan).

To investigate the intrinsic mechanism of the interfacial scavenging, the effects of large-scale defects such as grain boundaries and dislocations, which often facilitate incidental occurrence of resistive switching both in single crystals and epitaxial thin films,[27] should be eliminated. We thus used amorphous STO, which has recently been reported to have a uniform defect distribution and good resistive switching characteristics,[9] as the oxide layer in our test cell, and the thickness of STO was set to a relatively large value of 100 nm. STO is also known as a model material for defect migration with an established mechanism of mixed anionic–electronic conduction and a relatively high ionic conductivity for oxygen;[28,29] these properties are suitable for studying defect formation. In addition, STO has a large oxygen non-stoichiometry down to $SrTiO_{2.5}$,[29] which enables the investigation of the formation of a high concentration of defects without matrix decomposition. The amorphous nature and structural uniformity of the deposited STO layers were confirmed by TEM and X-ray diffraction using a D8 Discover (Bruker AXS Inc., Madison, WI, USA). In addition, the flatness of the surface of the deposited STO layer was confirmed using AFM, with a root mean square (rms) roughness of ~0.11 nm.

RESULTS AND DISCUSSION

Our STO films were highly insulating in the initial state, reflecting the absence of grain boundaries and dislocations. Figure 1a presents the typical *I–t* characteristics of the Pt/STO/Pt and Pt/M(10 nm)/STO/Pt structures with M = Ta and Ti, which were measured by applying

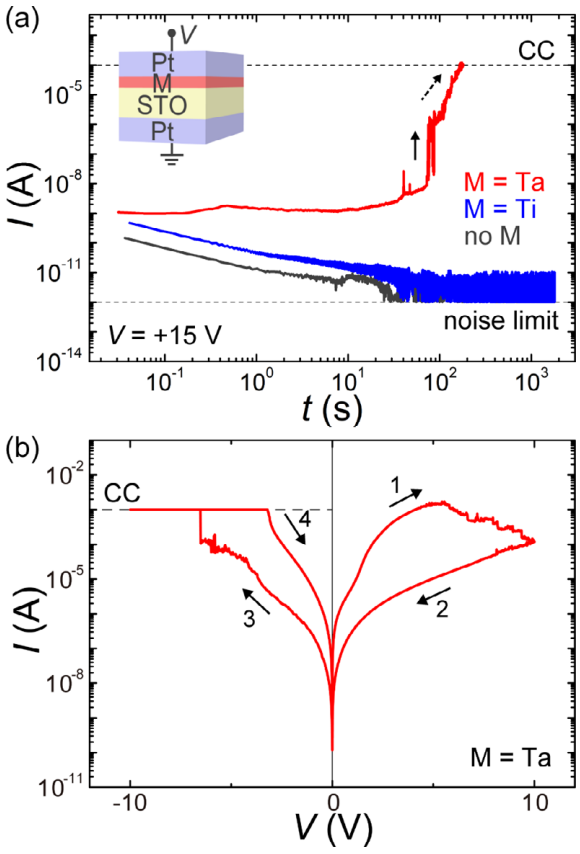

Figure 1. (a) *I–t* characteristics of Pt/STO/Pt and Pt/M(10 nm)/STO/Pt structures with M = Ti and Ta measured with the application of a constant voltage of V = +15 V. A CC of 0.1 mA was set by the measurement apparatus. The bottom broken line shows the error limit in the measurement determined by the cable noise (~1 pA). (b) *I–V* characteristics of Pt/Ta(10 nm)/STO/Pt structure measured after resistance decrease with voltage application of +10 V for 24 s. The arrows and numbers in (b) indicate the sequence of voltage sweeping.

constant voltages of +15 V. The Pt/STO/Pt structure, for which no scavenging layer was inserted, showed no change in resistance over a long measurement period of 30 min (Figure 1a). Note that the initial current decrease from ~0.1 nA to ~10 pA originates from the flow of transient

charging currents in the capacitor-like structure, with the current then gradually reaching the experimental measurement limit (~1 pA). The nature of the Pt/STO/Pt structures remained insulating even with the application of higher voltages up to ±30 V, independent of the bias polarity. We observed that the insertion of the Ti scavenging layer was not effective for reducing the device resistance. As observed in Figure 1a, most of the Pt/Ti(10 nm)/STO/Pt structures showed no resistance decrease in the *I–t* characteristics. Although Ti has been commonly used as a scavenging material in previous works, we only observed a resistance decrease in the Pt/Ti/STO/Pt structures in a limited number of samples accompanied by an incidental large increase in the current (Figure S1a). A similar abrupt current increase was also observed in the *I–t* characteristics of Pt/Al/STO/Pt and Pt/Zr/STO/Pt structures (Figure S1a).

However, when Ta was used as the scavenging metal, rather different behaviors were observed in the *I–t* characteristics, and resistance modulation of the STO layer became possible. In the *I–t* characteristics of the Pt/Ta/STO/Pt structure (Figure 1a), the coexistence of two types of resistance changes was observed. In the Pt/Ta/STO/Pt structure, abrupt current increases were also observed at 40 and 80 s (indicated by the solid arrow), similarly to other M layers. In addition, a gradual increase in current was observed for the Pt/Ta/STO/Pt structure over the measurement period of 180 s, as indicated by the dotted arrow. The currents in this structure finally reached the current compliance (CC) of 0.1 mA (set by the measurement apparatus), and persistent resistance decrease from the initial value of 10 GΩ to 10 MΩ was observed after reaching the CC. The gradual resistance change was only observed in structures with M = Ta and became more dominant at lower voltages (< +10 V). The abrupt type of resistance change was more often observed at $V \geq +15$ V (Figure S1a), and the height of the current jump also increased with increasing voltage. We confirmed that the resistance changes in the Pt/Ta/STO/Pt structure

could not be induced by applications of negative voltages (as demonstrated in Figure S1b for V = −15 V).

The bipolarity of the *I–t* characteristics suggests the occurrence of electrochemical oxidation of the Ta layer under positive bias voltages and resulting changes in the oxygen defect concentrations in the STO layer. An abrupt increase in the current has generally been observed in the *I–t* characteristics of various resistive switching materials.[27,30,31] The abrupt resistance changes have been attributed to the formation of conductive filamentary paths, and the involvement of the filament formation has been demonstrated for Ag/a-Si/W structures based on in situ TEM observation.[31] However, the gradual current increase observed for the Pt/Ta/STO/Pt structure is a less common phenomenon. We observed that the defect formation in the gradual current increase is rather non-local and occurs over a wide area of the interface, as discussed later.

The *I–V* characteristics of the Pt/STO/Pt and Pt/M/STO/Pt structures did not exhibit resistive switching behavior in the initial insulating state. Hysteretic *I–V* characteristics, which are a signature of the occurrence of defect-mediated resistive switching, were observed in the Pt/Ta/STO/Pt structures after appropriately reducing the resistance through the application of voltage with controlled amplitudes and times (Figure 1b). This finding confirmed that the Ta scavenging layer can generate a sufficient amount of oxygen defects for the induction of resistive switching effects in STO. In the structures with M = Al, Ti, and Zr, however, it was difficult to induce stable resistive switching because of the poor resistance controllability (easy hard breakdown by the abrupt current increase). When d was increased from 10 nm, a resistance decrease occurred at lower voltages in the Pt/Ta/STO/Pt structures, whereas no significant change in the *I–t* characteristics was observed for M = Al, Ti, and Zr. At d = 50 nm, however,

complete breakdown of the STO layer was easily induced for the Pt/Ta/STO/Pt structures in the voltage sweeping cycles. We can assume that both the use of an appropriate scavenging material and control of the relative thickness to oxide layer are of key importance for inducing stable resistive switching with a scavenging layer.

Figure 2a summarizes the voltage dependence of the yield ratio (r) of the resistance decrease in Pt/M(10 nm)/STO/Pt structures measured by applying positive constant voltages with various amplitudes. Here, the occurrence of the resistance decrease is defined by a current flow of ≥ 0.1 mA in the I–t measurements, and r represents the ratio of devices where the resistance decrease was observed in the 30-min I–t measurements. To statically evaluate the material dependence, 11–42 devices were measured for each data point in Figure 2a. The results reveal that the structure with the Ta layer had a higher yield of resistance decrease than the structures with Al, Ti, and Zr, which are popularly used scavenging metals. In the Pt/Ta/STO/Pt structures, nearly all the measured samples exhibited resistance changes under $V \geq +15$ V, suggesting their high oxygen scavenging efficiency. The Pt/STO/Pt structures showed no resistance decrease at any voltage, and the resistance decrease in the Pt/Ti/STO/Pt and Pt/Al/STO/Pt structures occurred in small numbers ($r \approx 30\%$) of samples at high voltages. In the Pt/Zr/STO/Pt structures, the resistance decrease was observed in a moderate number of samples with $r \approx 50\%$ at $V \geq +15$ V.

The switching time (t_{sw}) of the Pt/Ta/STO/Pt structures showed an exponential dependence on the applied voltage. Here, t_{sw} is defined as the time at which a current flow of ≥ 0.1 mA was observed for the first time in the I–t measurements. As observed in Figure 2b, t_{sw} of the Pt/Ta/STO/Pt structures exponentially decreased with increasing V. By prolonging the measurement time to >30 min, we also observed a resistance decrease of ≥ 0.1 mA at lower voltages of ≤ +10 V. In the structures with M = Al, Ti, and Zr, however, the V dependence of t_{sw}

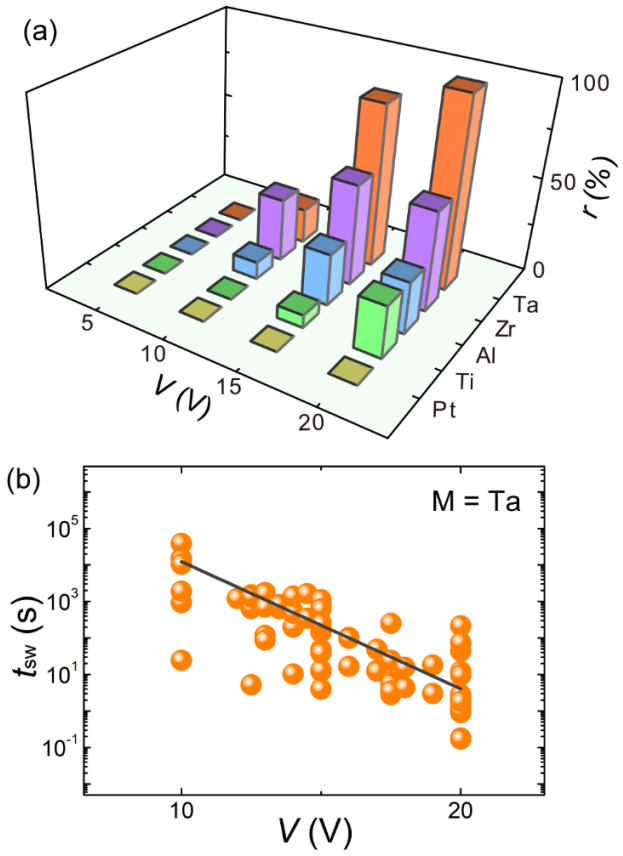

Figure 2. (a) Voltage dependence of r of resistance decrease (I > 0.1 mA) in Pt/M(10 nm)/STO/Pt structures with various M layers obtained from 30-min I–t measurements. (b) Voltage dependence of t_{sw} for Pt/Ta(10 nm)/STO/Pt structures.

became obscure (Figure S2). The exponential dependence of t_{sw} on V is known as an intrinsic behavior of resistive switching materials, where t_{sw} is predominated by a single limiting factor such as interfacial reactions,[32] defect nucleation,[32,33] and defect transport in the insulating layer.[30,32,34] The t_{sw}–V dependence observed for Pt/Ta/STO/Pt structures suggests that the defect formation in the structures is relatively homogeneous, whereas rather random defect formation is

suggested for the structures with M = Al, Ti, and Zr, resulting in contributions from multiple limiting factors and larger distributions of t_{sw}.

The active oxygen scavenging phenomenon observed for Ta layers cannot be explained by previous models based on the bulk thermodynamic parameters of scavenging materials. In previous studies,[10–12,14,15,18,20–22] oxygen scavenging effects have been understood based on the bulk reactivity of metals, with the formation free energy of the stable oxide per oxygen atom (ΔG°_{ox}: ΔG°/x for M + xO → MO_x + ΔG°) being used as the critical parameter for estimating the scavenging efficiency. However, this well-accepted model is not valid for our results because Ta has the largest ΔG°_{ox} among the materials used in this study (Table 1). The difference in r between the Pt/Al/STO/Pt and Pt/Zr/STO/Pt structures (Figure 2a) is also unexpected from ΔG°_{ox} because Al and Zr have similar ΔG°_{ox} values. The work function (ϕ) of the metal layer is recognized as a predominant parameter for interface-type resistive switching[39] and determines the Schottky barrier height at the metal/oxide interface.[40] However, we confirmed that Schottky barrier at the M/STO interface only has a small effect on the current transport of our structures from the *I–V* measurements (Figure S3). No clear relationship was also observed between ϕ and the measured r values (Table 1). The electronegativity (X) of the scavenging metal, which is a parameter related to ΔG°_{ox}, has recently been proposed as another possible factor contributing to the scavenging rate.[41] This model also fails to explain our observations because Ta has the largest X in the used materials. These facts suggest that the rate of oxygen scavenging reactions (or switching voltages and times for resistive switching devices) is not directly determined by these chemical parameters and that important contributions from the interfacial reaction behavior are involved in the actual process.

Table 1. ΔG°_{ox}, ϕ, and X of Scavenging Materials

materials	ΔG°_{ox} [kJ/mol][35,36]	ϕ [eV][37]	X[38]
Al	−526	4.28	1.5
Zr	−519	4.05	1.5
Ti	−441	4.33	1.6
Ta	−394	4.25	1.7
Pt	−82	5.65	2.1

To elucidate the origin of the unexpected material dependence of oxygen scavenging effects, structural characterizations of the scavenging layers were performed using HRTEM. TEM images of the Pt/Ta/STO/Pt and Pt/Ti/STO/Pt structures at the Pt/M/STO interfaces for the pristine samples are presented in Figure 3. Additional TEM observations confirmed that the STO layers in both structures were completely amorphous and uniform and that no structural randomness was observed even after resistance decrease resulting from the application of voltage. The Pt electrodes exhibited a polycrystalline structure in both structures, where lattice fringes assignable to the fcc structure of Pt were apparent. In the TEM images of the scavenging layers, however, clear structural differences were observed depending on the material. The Ta scavenging layers in the Pt/Ta/STO/Pt structures, where active oxygen scavenging was suggested, exhibited a highly uniform structure throughout the layer (Figures 3a and 3b). The Ta scavenging layer also formed a very flat interface with STO (Figure 3a). Figure 3c presents a fast Fourier transformation (FFT) pattern for the TEM image of the Ta scavenging layer, which corresponds to a defined part of Figure 3b. Only a diffuse halo pattern was observed in the FFT image, indicating the amorphous nature of the Ta scavenging layer. In addition, after inducing resistive

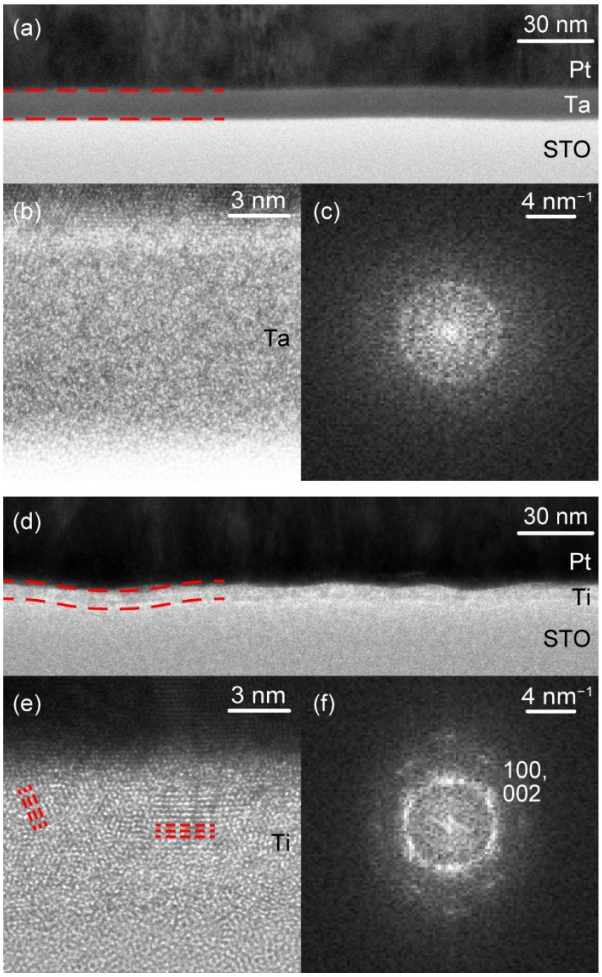

Figure 3. Cross-sectional TEM images of scavenging metal layers at different magnifications and their fast Fourier transformations in the scavenging layer part for (a–c) Pt/Ta(10 nm)/STO/Pt and (d–f) Pt/Ti(10 nm)/STO/Pt structures. The dashed lines in (a, d) and (e) are guides for the eye of the interfaces and lattice fringes, respectively.

switching with the application of V = +15 V, we observed that the Ta scavenging layers remained structurally uniform and amorphous. For the Ti scavenging layers, where the lowest r of resistive switching was obtained (Figure 2a), a very different structure was observed in the

TEM images. The structure of the Ti scavenging layer was polycrystalline and granular, and randomly oriented lattice fringes were observed in the layer (red dashed lines in Figure 3e). The FFT image of the Ti scavenging layer in Figure 3f exhibits a circularly distributed pattern of bright spots, confirming the polycrystalline nature of the layer. The brightest circular spots at approximately 4 nm^{-1} were assigned to 100 and 002 diffraction from the hcp structure of Ti metal. No significant diffraction peaks from oxidized TiO_x (e.g., peaks at 2.9 nm^{-1} for anatase or rutile TiO_2) were observed in the FFT image. Therefore, the Ti scavenging layer is considered to contain a significant amount of crystalline grains of non-oxidized Ti in contrast to the amorphous structure of the Ta layer. The granular growth of the Ti layer was also observed to affect the interfacial structure at the M/STO interface: a rough wavy interface was formed between the Ti and STO layers, as indicated by the red dashed lines in Figure 3d.

Figure 4 shows the AFM surface morphologies of the scavenging layers on STO. These layers were deposited on STO(100 nm)/Pt(100 nm)/Ti(10 nm)/SiO_2/Si structures under the same conditions as those for the samples for the transport and TEM measurements, without fabricating the Pt top electrodes. Note that the effect of oxidation from STO layers will be involved in the morphologies because we observed that the material underneath (STO, Pt, or SiO_2/Si) has a large effect on the morphology (data not shown). The morphologies of the M/STO structures revealed the presence of a clear material dependence of the scavenging metals. As shown in Figure 4a, the surface of the Ta scavenging layer was atomically smooth, with a very low rms surface roughness of 0.14 nm. For the surface of the Ti layers, however, a rough and granular morphology with an rms roughness of 0.79 nm was observed (Figure 4c). These observations for Ta and Ti layers are consistent with the corresponding TEM results for Pt/M/STO/Pt structures (Figure 3). The Zr scavenging layer had a moderately flat surface with rms = 0.25 nm (Figure

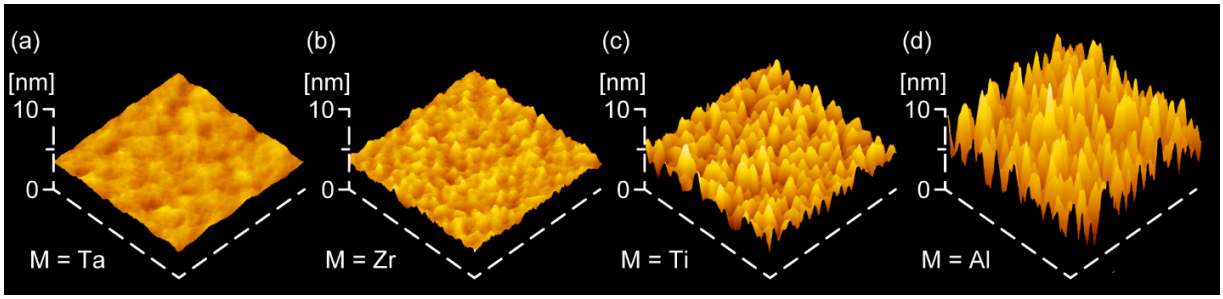

Figure 4. AFM topographic images of (a) Ta/STO/Pt, (b) Zr/STO/Pt, (c) Ti/STO/Pt, and (d) Al/STO/Pt surfaces with d = 10 nm. The scanned area is 1.0 μm × 1.0 μm.

4b), and a very rough structure with rms = 1.77 nm was observed for the surface of the Al scavenging layer (Figure 4d). The decreasing behaviors of the resistance under the application of voltage (Figure 2a) were correlated to the smoothness of the M layers (Figures 3 and 4). Relatively higher r was observed for the smooth scavenging materials (Ta and Zr), whereas lower r was observed for the rough scavenging materials (Ti and Al).

If the cation migration is not assisted by electric field application, oxidation of a metal film often results in an increase of the surface roughness depending on the material. This has been attributed to nonuniform progress of the oxidation resulting from the low oxygen diffusibility of the elemental metal and metal suboxide. If the internal cation migration and oxygen diffusion is insufficient, the metal film will be partly oxidized along the preferred orientations, and a sublattice structure with small surface energy [e.g., (110) of TiO_2 and (0001) of Al_2O_3] will be preferentially formed on the grain surface.[42,43] The formation of these preferentially oxidized planes often leads to a rough film structure, and a granular structure is generally formed in oxidized Ti and Al thin films.[43–45] Therefore, when Ti and Al are used as a scavenging layer,

structural coarsening may be inevitable. However, the structural roughness may be suppressed in Ta and Zr scavenging layers because they have high oxygen diffusibility in metal and metal suboxide states[46–49] and because relatively isotropic progress is expected for the oxidation. In fact, recent studies have demonstrated that formation of a highly smooth surface is possible for Ta and their alloys in the anodic oxidation of metal films.[50,51] The smooth structures observed in Figures 4a and 4b are consistent with this assumption and suggest the advantages of these metals in forming a flat metal/oxide junction.

The EDX results confirmed that the oxygen concentration in the STO layer decreased with the insertion of the Ta layer without the application of bias voltages (as shown in Figure S4). The occurrence of effective oxygen scavenging between Ta and STO was demonstrated for the pristine structures. In addition, we observed that the internal distribution of oxygen in the scavenging layers has a strong material dependence. EDX mapping of the oxygen K-line intensity and corresponding high-angle annular dark field scanning transmission electron microscopy (HAADF-STEM) images of the Pt/M/STO/Pt structures are presented in Figure 5 for the Pt/Ta(10 nm)/STO and Pt/Ti(10 nm)/STO interfaces. Figures 5a–5c reveal that a large amount of oxygen was distributed in the Ta scavenging layer at a significantly higher level than that in the Pt layer, and the distributions are rather uniform. This result indicates that the Ta layer was uniformly oxidized from the STO layer through the scavenging reactions. In the Ti scavenging layer, however, the internal oxygen distributions were non-uniform. The oxidation of the Ti layer was observed to occur only near the Pt/Ti and Ti/STO interfaces (Figure 5d and 5e). The EDX line profiles indicate that the middle part of the Ti layer had a very small oxygen concentration, comparable to that in the Pt layer (Figure 5f). Most of the Ti layer was thus

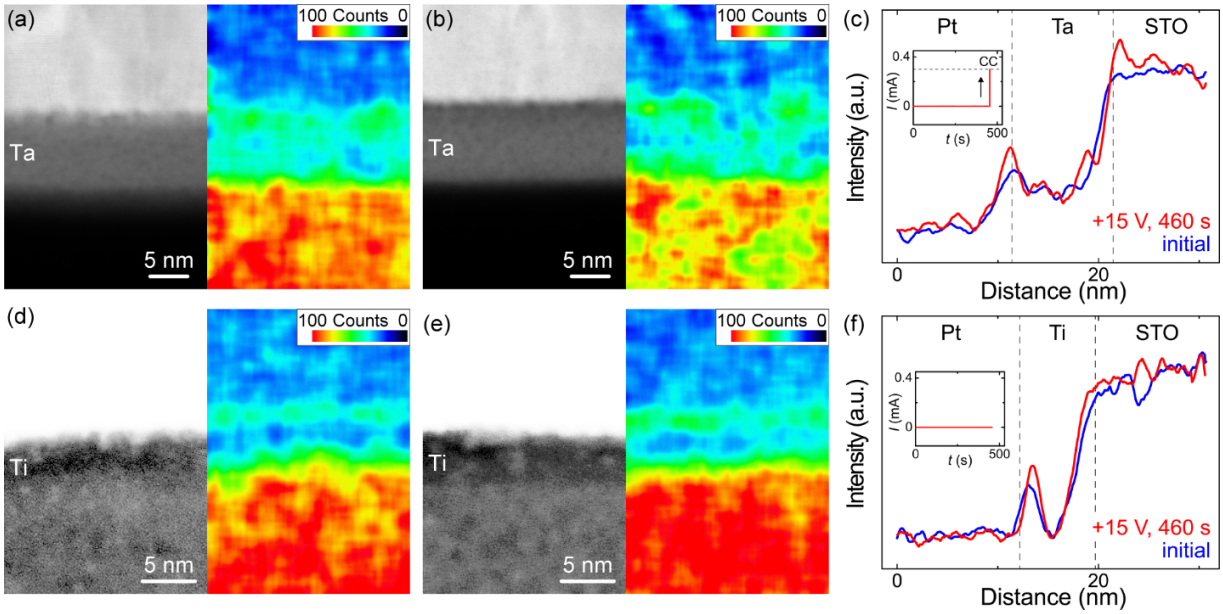

Figure 5. HAADF-STEM images (left panels) and corresponding EDX mappings of oxygen K-line intensity (right panels) for Pt/Ta(10 nm)/STO/Pt structure (a) in the initial state and (b) after abrupt resistance decrease after the application of $V = +15$ V for 460 s [inset in (c)] and Pt/Ti(10 nm)/STO/Pt structure (d) in the initial state and (e) after application of $V = +15$ V for 460 s [not switched, inset in (f)]. Line profiles of EDX oxygen K-line intensity across the (c) Pt/Ta/STO and (f) Pt/Ti/STO interfaces, which were averaged over 40 nm in the in-plane direction. The vertical dashed lines in (c) and (f) indicate the positions of the Pt/M and M/STO interfaces determined from EDX elemental analysis for Pt, Ti, and Ta.

considered to remain unoxidized, which is consistent with the polycrystalline TEM images (Figure 3e) and thickness independence of the *I*–*t* characteristics.

The difference in the oxygen distributions observed in the initial state indicates a large difference in the oxygen diffusibility of the Ta and Ti layers. The high oxygen diffusibility of the Ta layer

facilitates oxygen transport from STO to Ta and can be considered the origin of the activation of oxygen scavenging in the initial state. Recent studies have reported the very high oxygen diffusibility of TaO_x both in amorphous[48] and crystalline states[47,49] (3.5×10^{-17} m^2/s for crystalline TaO_x at room temperature). The high diffusibility of oxygen has been attributed to highly equivalent bonding energies of the Ta–O bondings, which permits easy exchange of oxygen ions[47–49]. The "adaptive" structure of TaO_x has thus been expected to enable long-range structural rearrangements of the Ta and O ions and active vacancy migration. The uniform structure (Figures 3 and 4) and oxygen distributions (Figures 5a and 5c) observed for our Ta layers are consistent with these theoretical models, and may demonstrate the advantage of such adaptive-structured materials in oxygen scavenging.

The effects of voltage application on vacancy formation were shown to depend on the type of resistance decrease observed in the structures. After abrupt resistance decrease with the application of a relatively high voltage of +15 V (inset of Figure 5c), little change was observed for the oxygen distributions in the Ta and STO layers (Figures 5c). Although such abrupt resistance decreases have been generally observed in resistive switching oxides with a filament-type mechanism,[27,30,31] our results suggest that a large change in the oxygen amount is not induced in this type of resistance change. Figures 5c and 5f show that a small increase of the oxygen amount is only induced at the Pt/Ta and Pt/Ti interfaces after the abrupt resistance decrease or equivalent voltage application. This finding indicates that oxygen ions attracted by positive voltages can arrive at the Pt electrodes through the M layers; however, the reactions with scavenging metals are not actively induced during the drift motion with a small ionic current.

We observed that the formation of a high concentration of oxygen defects is possible by inducing

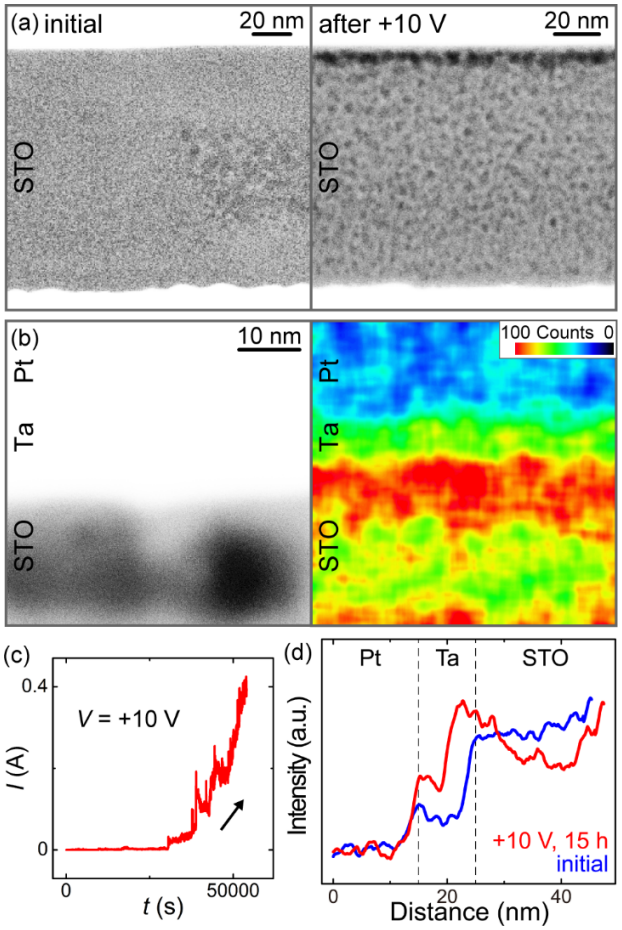

Figure 6. (a) HAADF-STEM images of Pt/Ta(10 nm)/STO/Pt structures in the initial state (left panel) and after gradual resistance decrease with the application of V = +10 V for 15 h (right panel). (b) HAADF-STEM image (left panel) and corresponding EDX mapping of oxygen K-line intensity (right panel) at the Pt/Ta/STO interface after the gradual resistance decrease. (c) I–t characteristics under a constant voltage of V = +10 V measured for the Pt/Ta(10 nm)/STO/Pt structure shown in (a) and (b). (d) Line profiles of EDX oxygen K-line intensity across the Pt/Ta/STO interfaces, which were averaged over 40 nm in the in-plane direction.

a gradual resistance decrease in Pt/Ta/STO/Pt structures using relatively low voltages. Figure 6a presents HAADF-STEM images of Pt/Ta(10 nm)/STO/Pt structures before and after the application of +10 V for 15 h. During the voltage application, a gradual increase of the current to 0.4 mA was observed in the *I*–*t* characteristics (Figure 6c). After the resistance decrease, a thin (~10 nm) region at the top of the STO layer darkened in the HAADF-STEM image (right panel of Figure 6a). EDX analysis (Figure 6b) indicated that these dark regions were deficient in oxygen compared with the surrounding STO. The contrast change in the HAADF-STEM image suggests that a large amount of oxygen defects was introduced into the STO layer with current flow as conductive defect clusters[52,53] and that the gradual resistance change was caused by the change in carrier concentrations. The oxygen concentration in the Ta layer showed a clear increase after the resistance decrease (Figure 6d). These results show that a large extent of redox reactions under bias voltages, reported for the electrode interfaces of resistive switching oxides,[23,24,54] was induced between our Ta and STO layers. The contrast change was not observed in the HAADF-STEM images after abrupt resistance decrease (Figure S5). Our results indicate that the use of an active scavenging metal and sufficiently long current flow time are essential for the formation of a high density of oxygen vacancies via electrochemical scavenging reactions.

The material dependence of oxygen scavenging and the effects of voltage application can be explained as follows (Figure 7). In the Ta scavenging layer with high oxygen diffusibility, the scavenged oxygen is uniformly distributed and a uniform layer of amorphous TaO_x is formed by the room-temperature oxidation in the initial state. A large amount of oxygen will be removed from the STO by the active oxygen diffusion in Ta, and the oxygen concentration of the STO layer will decrease without the application of voltage (Figure S4). A flat Ta/STO interface was

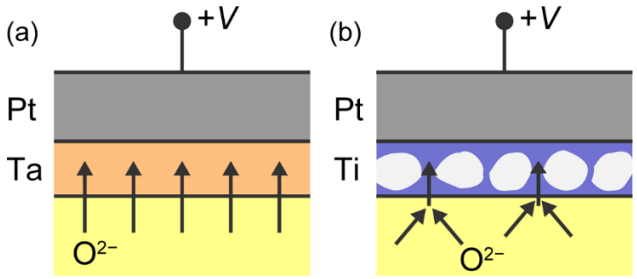

Figure 7. Schematic illustrations of oxygen scavenging processes in Pt/M/STO/Pt structures with M = (a) Ta and (b) Ti.

also formed because of the structural uniformity of TaO_x. When a Ti layer is used for oxygen scavenging, the scavenged oxygen is inhomogeneously distributed in the layer because of the low oxygen diffusibility. The scavenged oxygen mainly remains in a narrow region near the Ti/STO interface, and most of the layer becomes granular Ti because of the partial oxidation along the preferred orientations. The top Pt/Ti interface is partially oxidized from the grain boundary diffusion in the Ti layer or the diffusion of atmospheric oxygen through the Pt electrode.[55,56] The granular structure of Ti layer forms rough interfaces in the structure both at the Pt/Ti and Ti/STO interfaces.

Under the application of positive voltage, oxygen ions drift toward the top Pt electrode and the STO layer is electrochemically reduced. Recent studies have demonstrated that tantalum cations also significantly drift in TaO_x by voltage applications,[24,54] and the cation migrations facilitate the oxygen migrations and redox reactions in TaO_x. The shorter t_{sw} of the Pt/Ta/STO/Pt structures (Figures 2 and S2) suggests that the field-driven migration of oxygen is faster in Ta layers due to the help from the tantalum migrations. In addition, because the Ta/STO interface is flatter, the scavenging reactions may occur over the entire interface and the active area for

scavenging will be large in Pt/Ta/STO/Pt structures. The electrochemical scavenging reactions progress with current flow, and gradual decrease of the resistance (Figure 6c) is induced by the oxygen defect formation. The abrupt resistance decrease (Figures 5c and S1) is believed to occur with incidental formation of filamentary paths. The filament formation causes an electrical short-circuit of the structure and will stop the scavenging reactions without forming a large amount of defects. In Pt/Ti/STO/Pt structures, the field-driven migration of oxygen will be hindered by the poor migrations of titanium cations. The granular structure of the Ti layer suggests that oxygen drifts through the grain boundaries with the application of voltage (Figure 7b). The reduction of STO will locally occur near the grain boundaries, and filamentary paths are mainly formed by the application of voltage.

Our results showed that Ta can work as an effective scavenging material due to the active interfacial reactions.[23–25] Although it has been used less often for oxygen scavenging, the smoothness of the scavenging reactions may offer many advantages for resistive-switching-device applications, including fast switching time, low switching voltage, and high device yield. Moreover, the Ta scavenging layer can be used as a promising tool for the exploration of defect-mediated functions at metal/oxide junctions.[2–5] The use of a Ta interface layer will enable the fabrication of an ideally flat metal/oxide junction and large modulation of the carrier concentration at the interface. The interface carriers may cause large changes in the various interface properties, which are worthy of further exploration.

CONCLUSIONS

We observed the occurrence of active oxygen scavenging in a resistive switching oxide of STO with a Ta interface layer. The results revealed that ΔG°_{ox} of the scavenging metal is not the only dominant parameter in oxygen scavenging and that the oxygen diffusibility and mechanism of the interfacial reactions of the scavenging metal also plays a critical role in the process. In the electrical transport measurements for Pt/M/STO/Pt structures, clear resistance decrease was observed for the structures with M = Ta, where active cation motion has recently been demonstrated for the suboxide (TaO_x). Gradual control of the resistance was also achieved in Pt/Ta/STO/Pt structures. TEM/EDX and AFM investigations revealed the uniform structure and oxygen distribution of the Ta scavenging layer, which formed a very flat interface with STO. The formation of a high concentration of interfacial defects was also observed for Pt/Ta/STO/Pt structures with the application of voltage. These results provide important insight for future developments of resistive switching memory with reliable operation and help to extend the applications of oxygen scavenging phenomena to various oxide devices.

ASSOCIATED CONTENT

Supporting Information.

Supporting Information is available free of charge on the ACS Publications website.
I–t characteristics of Pt/STO/Pt and Pt/M/STO/Pt structures, voltage dependence of t_{sw}, *I–V* characteristics of Pt/STO/Pt and Pt/M/STO/Pt structures, oxygen distributions in STO/Pt, Pt/STO/Pt and Pt/Ta/STO/Pt structures, and HAADF-STEM images of Pt/Ta/STO/Pt structure after abrupt resistance decrease. (PDF)

AUTHOR INFORMATION

Corresponding Author

*E-mail: a.fukuchi@ist.hokudai.ac.jp (A.T.F.).

ORCID

Atsushi Tsurumaki-Fukuchi: 0000-0003-2529-8897

Notes

The authors declare no competing financial interest.

ACKNOWLEDGMENTS

Part of this work was financially supported under KAKENHI by the Japan Society for the Promotion of Science (JSPS) (Nos. 16K18073, 16H04339, 15H01706). The Nippon Sheet Glass Foundation for Materials Science and Engineering and Scholar Project of Toyota Physical and Chemical Research Institute are also acknowledged for their financial support of this work. The experiments were partly performed under the Nanotechnology Platform Program (Hokkaido Univ.) organized by the Ministry of Education, Culture, Sports, Science and Technology (MEXT), Japan. We also thank Tiffany Jain, M.S., from Edanz Group (www.edanzediting.com/ac) for editing a draft of this manuscript.

REFERENCES

(1) Picone, A.; Riva, M.; Brambilla, A.; Calloni, A.; Bussetti, G.; Finazzi, M.; Ciccacci, F.; Duò, L.; Reactive Metal–Oxide Interfaces: A Microscopic View. *Surf. Sci. Rep.* **2016**, *71*, 32–76.

(2) Li, Y. Y.; Wang, Q. X.; An, M.; Li, K.; Wehbe, N.; Zhang, Q.; Dong, S.; Wu, T. Nanoscale Chemical and Valence Evolution at the Metal/Oxide Interface: A Case Study of Ti/$SrTiO_3$. *Adv. Mater. Interfaces* **2016**, *3* (17), 1600201.

(3) Veal, B. W.; Kim, S. K.; Zapol, P.; Iddir, H.; Baldo, P. M., Eastman, J. A. Interfacial Control of Oxygen Vacancy Doping and Electrical Conduction in Thin Film Oxide Heterostructures. *Nat. Commun.* **2016**, *7*, 11892.

(4) Bauer, U.; Yao, L.; Tan, A. J.; Agrawal, P.; Emori, S.; Tuller, H. L.; Dijken, S. V.; Beach, G. S. D. Magneto-Ionic Control of Interfacial Magnetism. *Nat. Mater.* **2015**, *14*, 174–181.

(5) Gilbert, D. A.; Olamit, J.; Dumas, R. K.; Kirby, B. J.; Grutter, A. J.; Maranville, B. B.; Arenholz, E.; Borchers, J. A.; Liu, K. Controllable Positive Exchange Bias via Redox-Driven Oxygen Migration. *Nat. Commun.* **2016**, *7*, 11050.

(6) Sawa, A. Resistive Switching in Transition Metal Oxide. *Mater. Today* **2008**, *11* (6), 28–36.

(7) Waser, R.; Dittmann, R.; Staikov, G.; Szot, K. Redox-Based Resistive Switching Memories – Nanoionic Mechanisms, Prospects, and Challenges. *Adv. Mater.* **2009**, *21* (25–26), 2632–2663.

(8) Yang, J. J.; Strukov, D. B.; Stewart, D. R. Memristive Devices for Computing. *Nat. Nanotechnol.* **2013**, *8*, 13–24.

(9) Nili, H.; Walia, S.; Balendhran, S.; Strukov, D. B.; Bhaskaran, M.; Sriram, S. Nanoscale Resistive Switching in Amorphous Perovskite Oxide (*a*-$SrTiO_3$) Memristors. *Adv. Funct. Mater.* **2014**, *24* (43), 6741–6750.

(10) Guox, L.; Fantini, A.; Chen, Y. Y.; Redolfi, A.; Degraeve, R.; Jurczak, M. Evidences of Electrode-Controlled Retention Properties in Ta_2O_5-Based Resistive Switching Memory Cells. *ECS Solid State Lett.* **2014**, *3* (11), Q79–Q81.

(11) Guo, Y.; Robertson, J. Materials Selection for Oxide-Based Resistive Random Access Memories. *Appl. Phys. Lett.* **2014**, *105* (22), 223516.

(12) Guo, Y.; Robertson, J. Ab Initio Calculations of Materials Selection of Oxides for Resistive Random Access Memories. *Microelectron. Eng.* **2015**, *147*, 339–343.

(13) Zhong, X.; Rungger, I.; Zapol, P.; Nakamura, H.; Asai, Y.; Heinonen, O. The Effect of a Ta Oxygen Scavenger Layer on HfO_2-Based Resistive Switching Behavior: Thermodynamic Stability, Electronic Structure, and Low-Bias Transport. *Phys. Chem. Chem. Phys.* **2016**, *18* (10), 7502–7510.

(14) Kim, W.; Menzel, S.; Wouters, D. J.; Guo, Y.; Robertson, J.; Roesgen, B.; Waser, R.; Rana, V. Impact of Oxygen Exchange Reaction at the Ohmic Interface in Ta_2O_5-Based ReRAM Devices. *Nanoscale* **2016**, *8* (41), 17774–17781.

(15) Celano, U.; Op de Beeck, J.; Clima, S.; Luebben, M.; Koenraad, P. M.; Goux, L.; Valov, I.; Vandervorst, W. Direct Probing of the Dielectric Scavenging-Layer Interface in Oxide Filamentary-Based Valence Change Memory. *ACS Appl. Mater. Interfaces* **2017**, *9* (12), 10820–10824.

(16) Hu, C.; McDaniel, M. D.; Posadas, A.; Demkov, A. A.; Ekerdt, J. G.; Yu, E. T. Highly Controllable and Stable Quantized Conductance and Resistive Switching Mechanism in Single-crystal TiO_2 Resistive Memory on Silicon. *Nano Lett.* **2014**, *14* (8), 4360–4367.

(17) Prezioso, M.; Merrikh-Bayat, F.; Hoskins, B. D.; Adam, G. C.; Likharev, K. K.; Strukov, D. B. Training and Operation of an Integrated Neuromorphic Network Based on Metal-Oxide Memristors. *Nature* **2015**, *521*, 61–64.

(18) Jeong, H. Y.; Lee, J. Y.; Choi, S. Y. Interface-Engineered Amorphous TiO_2-Based Resistive Memory Devices. *Adv. Funct. Mater.* **2010**, *20* (22), 3912–3917.

(19) Kim, S.; Jeong, H. Y.; Kim, S. K.; Choi, S. Y.; Lee, K. J. Flexible Memristive Memory Array on Plastic Substrates. *Nano Lett.* **2011**, *11* (12), 5438–5442.

(20) Lee, C. B.; Kang, B. S.; Benayad, A.; Lee, M. J.; Ahn, S.-E.; Kim, K. H.; Stefanovich, G.; Park, Y.; Yoo, I. K. Effects of Metal Electrodes on the Resistive Memory Switching Propety of NiO Thin Films. *Appl. Phys. Lett.* **2008**, *93* (4), 042115.

(21) Liao, Z. L.; Wang, Z. Z.; Meng, Y.; Liu, Z. Y.; Gao, P.; Gang, J. L.; Zhao, H. W.; Liang, X. J.; Bai, X. D.; Chen, D. M. Categorization of Resistive Switching of Metal-$Pr_{0.7}Ca_{0.3}MnO_3$-Metal Devices. *Appl. Phys. Lett.* **2009**, *94* (25), 253503.

(22) Lin, K. L.; Hou, T. H.; Shieh, J.; Lin, J. H.; Chou, C. T.; Lee, Y. J. Electrode Dependence of Filament Formation in HfO_2 Resistive-Switching Memory. *J. Appl. Phys.* **2011**, *109* (8), 084104.

(23) Lübben, M.; Karakolis, P.; Ioannour-Sougleridis, V.; Normand, P.; Dimitrakis, P.; Valov, I. Graphene-Modified Interface Controls Transition from VCM to ECM Switching Modes in Ta/TaO_x Based Memristive Devices. *Adv. Mater.* **2015**, *27* (40), 6202–6207.

(24) Wedig, A.; Luebben, M.; Cho, D.-Y.; Moors, M.; Skaja, K.; Rana, V.; Hasegawa, T.; Adepalli, K. K.; Yildiz, B.; Waser, R.; Valov, I. Nanoscale Cation Motion in TaO_x, HfO_x and TiO_x Memristive Systems. *Nat. Nanotechnol.* **2016**, *11*, 67–74.

(25) Cho, D.-Y.; Luebben, M.; Wiefels, S.; Lee, K.-S.; Valov, I. Interfacial Metal–Oxide Interactions in Resistive Switching Memories. *ACS Appl. Mater. Interfaces* **2017**, *9* (22), 19287–19295.

(26) Valov, I. Interfacial Interactions and Their Impact on Redox-Based Resistive Switching Memories (ReRAMs). *Semicond. Sci. Technol.* **2017**, *32* (9), 093006.

(27) Szot, K.; Speier, W.; Bihlmayer, G.; Waser, R. Switching the Electrical Resistance of Individual Dislocations in Single-Crystalline $SrTiO_3$. *Nat. Mater.* **2006**, *5*, 312–320.

(28) Messerschmitt, F.; Kubicek, M.; Schweiger, S.; Rupp, J. L. M. Memristor Kinetics and Diffusion Characteristics for Mixed Anionic-Electronic $SrTiO_{3-\delta}$ Bits: The Memristor-Based Cottrell Analysis Connecting Material to Device Performance. *Adv. Funct. Mater.* **2014**, *24* (47), 7448–7460.

(29) Messerschmitt, F.; Kubicek, M.; Rupp, J. L. M. How Does Moisture Affect the Physical Property of Memristance for Anionic-Electronic Resistive Switching Memories? *Adv. Funct. Mater.* **2015**, *25* (32), 5117–5125.

(30) Tsuruoka, T.; Terabe, K.; Hasegawa, T.; Aono, M. Forming and Switching Mechanisms of a Cation-Migration-Based Oxide Resistive Memory. *Nanotechnology* **2010**, *21* (42), 425205.

(31) Yang, Y.; Gao, P.; Gaba, S.; Chang, T.; Pan, X.; Lu, W. Observation of Conducting Filament Growth in Nanoscale Resistive Memories. *Nat. Commun.* **2012**, *3*, 732.

(32) Menzel, S.; Tappertzhofen, S.; Waser, R.; Valov, I. Switching Kinetics of Electrochemical Metallization Memory Cells. *Phys. Chem. Chem. Phys.* **2013**, *15* (18), 6945–6952.

(33) Valov, I.; Staikov, G. Nucleation and Growth Phenomena in Nanosized Electrochemical Systems for Resistive Switching Memories. *J. Solid State Electrochem.* **2013**, *17* (2), 365–371.

(34) Jo, S. H.; Kim, K. H.; Lu, W. Programmable Resistance Switching in Nanoscale Two-Terminal Devices. *Nano Lett.* **2009**, *9* (1), 496–500.

(35) Samsonov, G. V. *The Oxide Handbook*; IFI/Plenum: New York, 1973.

(36) Birks, N.; Meier, G. H.; Pettit, F. S. *Introduction to the High-temperature Oxidation of Metals*, 2nd ed; Cambridge University Press: Cambridge, 2006, http://www.doitpoms.ac.uk/tlplib/ellingham_diagrams/interactive.php.

(37) Michaelson, H. B. The Work Function of the Elements and Its Periodicity. *J. Appl. Phys.* **1977**, *48* (11), 4729–4733.

(38) Gordy, W.; Thomas, W. J. O. Electronegativities of the Elements. *J. Chem. Phys.* **1956**, *24* (2), 439–444.

(39) Sawa, A.; Fujii, T.; Kawasaki, M.; Tokura, Y. Hysteretic Current–Voltage Characteristics and Resistance Switching at a Rectifying Ti/$Pr_{0.7}Ca_{0.3}MnO_3$ Interface. *Appl. Phys. Lett.* **2004**, *85* (18), 4073–4075.

(40) Robertson, J. Band Offsets, Schottky Barrier Heights, and Their Effects on Electronic Devices. *J. Vac. Sci. Technol. A* **2013**, *31* (5), 050821.

(41) Kim, J.; Inamdar, A. I.; Jo, Y.; Woo, H.; Cho, S.; Pawar, S. M.; Kim, H.; Im, H. Effect of Electronegativity on Bipolar Resistive Switching in a WO_3-Based Asymmetric Capacitor Structure. *ACS Appl. Mater. Interfaces* **2016**, *8* (14), 9499–9505.

(42) Ma, F.; Zhang, J. M.; Xu, K. W. Surface-Energy-Driven Abnormal Grain Growth in Cu and Ag Films. *Appl. Surf. Sci.* **2005**, *242* (1–2), 55–61.

(43) Ting, C. C.; Chen, S. Y.; Liu, D. M. Preferential Growth of Thin Rutile TiO_2 upon Thermal Oxidation of Sputtered Ti Films. *Thin Solid Films* **2002**, *402* (1–2), 290–295.

(44) Zeman, P.; Takabayashi, S. Effect of Total and Oxygen Partial Pressures on Structure of Photocatalytic TiO_2 Films Sputtered on Unheated Substrate. *Surf. Coat. Technol.* **2002**, *153* (3), 93–99.

(45) Qiu, H.; Wang, F.; Wu, P.; Pan, L.; Li, L.; Xiong, L.; Tian, Y. Effect of Deposition Rate on Structural and Electrical Properties of Al Films Deposited on Glass by Electron Beam Evaporation. *Thin Solid Films* **2002**, *414* (1), 150–153.

(46) Li, H.; Liang, K.; Gu, S.; Xiao, G. Orientated Nano-Structured ZrO_2 Thin Films on Fused Quartz Substrate by Sol-Gel Process. *J. Mater. Sci. Lett.* **2001**, *20* (14), 1301–1303.

(47) Guo, Y.; Robertson, J. Oxygen Vacancy Defects in Ta_2O_5 Showing Long-Range Atomic Re-Arrangements. *Appl. Phys. Lett.* **2014**, *104* (11), 112906.

(48) Nakamura, R.; Toda, T.; Tsukui, S.; Tane, M.; Ishimaru, M.; Suzuki, T.; Nakajima, H. Diffusion of Oxygen in Amorphous Al_2O_3, Ta_2O_5, and Nb_2O_5. *J. Appl. Phys.* **2014**, *116* (3), 033504.

(49) Jiang, H.; Stewart, D. A. Enhanced Oxygen Vacancy Diffusion in Ta_2O_5 Resistive Memory Devices Due to Infinitely Adaptive Crystal Structure. *J. Appl. Phys.* **2016**, *119* (13), 134502.

(50) Zaffora, A.; Santamaria, M.; Di Franco, F.; Habazaki, H.; Di Quarto, F. Photoelectrochemical Evidence of Nitrogen Incorporation during Anodizing Sputtering-Deposited Al-Ta Alloys. *Phys. Chem. Chem. Phys.* **2016**, *18* (1), 351–360.

(51) Zaffora, A.; Cho, D.-Y.; Lee, K.-S.; Di Quarto, F.; Waser, R.; Santamaria, M.; Valov, I. Electrochemical Tantalum Oxide for Resistive Switching Memories. *Adv. Mater.* **2017**, *29* (43), 1703357.

(52) Muller, D. A.; Nakagawa, N.; Ohtomo, A.; Grazul, J. L.; Hwang, H. Y. Atomic-Scale Imaging of Nanoengineered Oxygen Vacancy Profiles in $SrTiO_3$. *Nature* **2004**, *430*, 657–661.

(53) Nili, H.; Ahmed, T.; Walia, S.; Ramanathan, R.; Kandjani, A. E.; Rubanov, S.; Kim, J.; Kavehei, O.; Bansal, V.; Bhaskaran, M.; Sriram, S. Microstructure and Dynamics of Vacancy-Induced Nanofilamentary Switching Network in Donor Doped $SrTiO_{3-x}$ Memristors. *Nanotechnology* **2016**, *27* (50), 505210.

(54) Moors, M.; Adepalli, K. K.; Lu, Q,; Wedig, A.; Bäumer, C.; Skaja, K.; Arndt, B.; Tuller, H. L.; Dittmann, R.; Waser, R.; Yidiz, B.; Valov, I. Resistive Switching Mechanisms on TaO_x and $SrRuO_3$ Thin-Film Surfaces Probed by Scanning Tunneling Microscopy. *ACS Nano* **2016**, *10* (1), 1481–1492.

(55) Schmiedl, R.; Demuth, V.; Lahnor, P.; Godehardt, H.; Bodschwinna, Y.; Harder, C.; Hmmer, L.; Strunk, H.-P.; Schulz, M.; Heinz, K. Oxygen Diffusion through Thin Pt Films on Si(100). *Appl. Phys. A* **1996**, *62*, 223–230.

(56) Jeong, H. Y.; Kim, S. K.; Lee, J. Y.; Choi, S.-Y. Role of Interface Reaction on Resistive Switching of Metal/Amorphous TiO_2/Al RRAM Devices. *J. Electrochem. Soc.* **2011**, *158* (10), H979–H982.

TABLE OF CONTENTS GRAPHIC

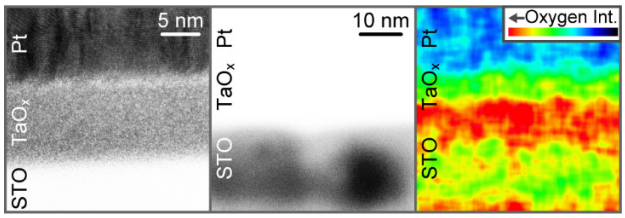

For Table of Contents Only